

NACA RM A54117

6439



RESEARCH MEMORANDUM

A FLIGHT INVESTIGATION AT TRANSONIC SPEEDS AND SMALL ANGLES
OF ATTACK OF THE AERODYNAMIC CHARACTERISTICS OF A MODEL
HAVING A 45° SWEEPBACK WING OF ASPECT RATIO 3
WITH AN NACA 64A006 AIRFOIL SECTION

By George H. Holdaway

Ames Aeronautical Laboratory
Moffett Field, Calif.

Classification and (or) changed to Unclassified
By Nasa Tech Pub Announcement #120
(OFFICIAL PUBLIC RELEASE CHANGE)

By 30557
NK

GRADE OF OFFICER MAKING CHANGE)
3D Man. 6.1
DATE

**NATIONAL ADVISORY COMMITTEE
FOR AERONAUTICS**

WASHINGTON

January 25, 1955



0143372

1U

NACA RM A54117

NATIONAL ADVISORY COMMITTEE FOR AERONAUTICS

RESEARCH MEMORANDUM

A FLIGHT INVESTIGATION AT TRANSONIC SPEEDS AND SMALL ANGLES
OF ATTACK OF THE AERODYNAMIC CHARACTERISTICS OF A MODEL
HAVING A 45° SWEPTBACK WING OF ASPECT RATIO 3
WITH AN NACA 64A006 AIRFOIL SECTION

By George H. Holdaway

SUMMARY

An investigation of the longitudinal aerodynamic characteristics of a model having a 45° sweptback wing of aspect ratio 3 and a 45° sweptback cruciform tail was made at transonic speeds and small angles of attack by a free-fall recoverable-model technique. The wing had NACA 64A006 airfoil sections perpendicular to the line of their own quarter chords. Load distributions on the fuselage in the vicinity of the wing and aerodynamic characteristics of the exposed wing panels were also determined. The Mach number range covered was $M = 0.88$ to $M = 1.12$ with resulting Reynolds numbers of 6,700,000 to 13,400,000 based on the wing mean aerodynamic chord.

The results showed trends in general agreement with wind-tunnel tests at higher and lower Mach numbers for a thinner wing of similar plan form. For the position of the horizontal tail tested (in the wing chord plane), its contribution to longitudinal stability was small for the high subsonic Mach numbers; increased tail effectiveness at the supersonic Mach numbers produced a large rearward shift of the aerodynamic center for the total configuration. The general level of the damping-in-pitch factor ($C_{m_q} + C_{m_{\dot{\alpha}}}$) was in agreement with predictions which attribute most of the contribution to longitudinal damping to the horizontal tail surfaces.

INTRODUCTION

As part of a general investigation of the characteristics of low-aspect-ratio swept wings, tests have been conducted in wind tunnels at subsonic and supersonic speeds on a wing having 45° of sweep and an aspect ratio of 3 (refs. 1 and 2). The present investigation was carried out to obtain the characteristics of a wing of similar plan form in the transonic Mach number range.

CONFIDENTIAL

A free-fall recoverable-model technique was used to obtain the transonic data. The tests were conducted at Mach numbers from $M = 0.88$ to $M = 1.12$; the corresponding Reynolds numbers were 6,700,000 to 13,400,000, respectively. Lift, drag, and pitching-moment coefficients were obtained for the total configuration (wing-body-tail combination) as well as for the exposed wing panels. The load distribution between wing and fuselage and the dynamic characteristics of the total configuration were also determined. As the result of loss of the model early in the program, the angle-of-attack range was limited from -1° to $+3^\circ$ with peak values ranging from -4° to $+5-1/2^\circ$.

The tests were made by the Ames Aeronautical Laboratory using the facilities of the NACA High-Speed Flight Research Station.

SYMBOLS

A	aspect ratio, $\frac{b^2}{S}$
a	speed of sound
b	wing span
C_D	drag coefficient for total configuration, $\frac{\text{drag}}{q_0 S}$
C_L	lift coefficient for total configuration, $\frac{\text{lift}}{q_0 S}$
$C_{L\alpha}$	lift-curve slope, $\frac{\partial C_L}{\partial \alpha}$
C_m	pitching-moment coefficient for total configuration about the model center of gravity, $\frac{\text{pitching moment}}{q_0 S \bar{c}}$
$C_{m\bar{c}/4}$	wing pitching-moment coefficient about the lateral axis through the quarter-chord point $\left(\frac{\bar{c}}{4}\right)$, $\frac{\text{pitching moment}}{q_0 S \bar{c}}$
C_{mq}	$\frac{\partial C_m}{\partial (q \bar{c} / 2V)}$

CONFIDENTIAL

$$C_{m\dot{\alpha}} \quad \frac{\partial C_m}{\partial (\dot{\alpha} \bar{c} / 2V)}$$

$$\bar{c} \quad \text{complete-wing mean aerodynamic chord, } \frac{\int_0^{b/2} c^2 dy}{\int_0^{b/2} c dy}$$

c local chord measured parallel to plane of symmetry

c' local chord of the design airfoil sections

M Mach number, $\frac{V}{a}$

$p_l - p_u$ difference in static pressure between lower and upper surface at a fuselage station

q angular velocity in pitch

q_o dynamic pressure, $\frac{1}{2} \rho V^2$

R Reynolds number based upon \bar{c}

S complete-wing area

t time

V free-stream velocity

y spanwise coordinate normal to plane of symmetry

α angle of attack of longitudinal axis of model

$$\dot{\alpha} \quad \frac{d\alpha}{dt}$$

CONFIDENTIAL

ρ mass density of air

$\frac{\partial P}{\partial \alpha}$ load-coefficient slope, $\frac{(P_L - P_U)_{\alpha_2} - (P_L - P_U)_{\alpha_1}}{(\alpha_2 - \alpha_1) q_0}$

Subscripts

- E aerodynamic coefficients (C_L , C_D , and $C_{m_{c/4}}$) based on exposed-wing loads and complete-wing area
- O zero-lift conditions when used with drag coefficients
- W aerodynamic coefficients (C_L , C_D , and $C_{m_{c/4}}$) based on exposed wing loads plus component of load over fuselage in the vicinity of the wing, and complete wing area

MODEL

The details of the wing, body, and tail are given in figure 1 and table I, and a photograph of the model in flight is presented in figure 2. The equation in figure 1 for the fuselage radii up to station 139.4 is for a fineness-ratio-12 Sears-Haack body. The radii for the remaining portion of the fuselage are given in table I.

The test wing had an aspect ratio of 3, a leading-edge sweepback of 45° , a taper ratio of 0.4, and NACA 64A006 airfoil sections perpendicular to the line of their own quarter chords. This quarter-chord line ($c'/4$) had a sweepback of 39.45° . The wing had no twist, dihedral, or incidence, and was of solid aluminum alloy construction. The wing-root fuselage juncture was sealed with a flexible rubber seal.

The instrumentation was identical with that described in reference 3 which also gives details of the wing balance and the wing seal mentioned previously. The locations of the pressure orifices are shown in figure 1(b).

TESTS

The test procedure consisted of releasing the model from a carrier airplane at an altitude of 40,000 feet, and allowing it to fall freely

without propulsion. When the desired Mach number was reached, the horizontal stabilizer was pulsed at 2.4-second intervals to produce oscillatory disturbances of about $\pm 4^\circ$ about the trim angle of attack. The pulses were terminated at a time calculated to permit the recovery of the model at a safe altitude. For this model, tests were made only about a trim angle of attack of 0° due to model destruction on the second drop.

The flight covered a Mach number range of $M = 0.88$ to $M = 1.12$ with a corresponding Reynolds number range of 6,700,000 to 13,400,000 (fig. 3). The range of angles of attack covered was -1° to $+3^\circ$; peak values ranging from -4° to $+5\frac{1}{2}^\circ$ were not included in the final data plots due to the scarcity of data at these angles (see ref. 3 for method of fairing data). The total configuration data obtained during control motion are not presented.

The instrument precision was generally the same as that of reference 3. The one exception was the reduced accuracy of the drag of the total configuration due to a reduced input voltage to the longitudinal accelerometer (at $M = 0.90$, accuracy believed to be within $C_D = \pm 0.005$ and at $M = 1.10$, $C_D = \pm 0.002$).

DATA REDUCTION

Complete information on data-reduction and computing methods used in this investigation has been presented in references 3 and 4, which present results from earlier investigations using the same flight-test technique. The following statements summarize the procedures used. The coefficients for the total configuration and the exposed wings were determined directly from corrected accelerometer and wing-balance records. The complete-wing coefficients were determined by combining the exposed-wing data with pressure data on the fuselage in the vicinity of the wing. In the case of the complete-wing drag coefficients, the data were obtained by adding the following three components of drag: exposed-wing drag, integrated fuselage pressures times the sine of the angle of attack, and friction drag of the fuselage (in the vicinity of the wing) assuming a friction-drag coefficient of 0.0025 for the average local Reynolds number of the tests.

The final results were evaluated from time histories of the coefficients which were then read at constant angles of attack and the results faired on Mach number cross plots. Typical data are presented and discussed in reference 3. Less scatter in the data of this investigation occurred, due to the small angle-of-attack range. The data for the total configuration were not evaluated during control motion, therefore these data are not presented at a Mach number of 0.9 at which time the initial pulse of the control was made.

RESULTS AND DISCUSSION

Lift

Curves of lift coefficients plotted against angles of attack for the test Mach number range are presented in figure 4 for the total configuration, the complete wing, and the exposed wing panels. These curves are quite linear which permitted the determination of lift-curve slopes, $C_{L\alpha}$, even though the angle-of-attack range was small. The lift-curve slopes are plotted in figure 5 as a function of Mach number, together with tunnel data (ref. 2) for a wing of the same plan form with a fuselage. The biconvex airfoil section of the tunnel model had a streamwise maximum-wing-thickness to chord ratio of 3 percent which is less than the corresponding value of about 5.1 percent for the wing of this investigation (NACA 64A006 airfoil section perpendicular to the quarter-chord line). The data of reference 1 are not presented because the results were preliminary. The subsonic data of reference 1 were corrected for reference 2 after a more complete static-pressure survey of the tunnel was made; therefore, the tabulated results presented in reference 2 were used to make comparisons with flight data. The lift-curve slopes for the complete wing are in reasonable agreement with the values from reference 2 at the higher subsonic speeds, but appear to be somewhat low at Mach numbers near 1.1.

Drag

Curves of drag coefficients plotted against angles of attack for the test Mach number range are presented in figure 6 for the total configuration, the complete wing, and the exposed wing panels. The zero-lift drag coefficients as a function of Mach number are presented in figures 7 and 8. The total-configuration data are presented in figure 7 together with the theoretical wave-drag coefficients, computed by the method of reference 6. The experimental drag coefficients at subsonic speeds were used to establish the datum above which the theoretical wave-drag coefficients were plotted. Reasonably good agreement between theory and experiment was obtained. The experimental zero-lift drag coefficients for the several components of the test model are presented in figure 8.

The variation of the drag-rise parameter ($\partial C_{DW} / \partial C_{LW}^2$) for the complete wing is compared with two theoretical curves in figure 9. In general, the results occupy a position about midway between the theoretical

values representing (1) an elliptical spanwise distribution of lift at subsonic speeds ($1/\pi A$), and (2) the resultant force vector perpendicular to the wing chord ($\frac{1}{57.3} C_{L\alpha_W}$, where $C_{L\alpha_W}$ is from the experimental data).

Static Longitudinal Stability

Pitching-moment coefficients are plotted in figure 10 as a function of the lift coefficients for the test Mach number range for the total configuration, complete wing, and exposed wing panels. The pitching-moment coefficients for the total configuration were computed by the angular accelerometer method which is described in an appendix of reference 3.

The aerodynamic-center positions near zero lift are presented in figure 11 as a function of Mach number for the total configuration, the complete wing, and the exposed wing panels. The data from figure 10(a), for the total configuration, were converted from moments about the center of gravity to moments about $\bar{c}/4$ to obtain one of the curves of figure 11. For comparison, the aerodynamic-center positions for the total configuration were also computed from the model period data by the method of reference 4. These values of aerodynamic-center position for the total configuration determined from period data were in approximate agreement with the values obtained from the angular accelerometer data of figure 10(a). The data of figure 11 indicate that the tail contribution to stability of the total configuration was small for Mach numbers near $M = 0.9$; however, increasing the Mach number from 0.9 to 1.1 produced an increase in tail effectiveness and a consequent large rearward shift of the aerodynamic center for the total configuration amounting to about $0.25 \bar{c}$.

No unusual characteristics were noted in the transonic speed range for the aerodynamic-center shift for the complete wing or exposed wing panels. Included in figure 11 are wind-tunnel data from reference 2 for the wing of reference 1. The pitching-moment curves plotted from the tabulated data of reference 2 were nonlinear at subsonic speeds, so the aerodynamic-center positions were estimated for two angle-of-attack ranges near zero lift, $\alpha = \pm 1/2^\circ$ and $\alpha = \pm 1^\circ$. The shift in aerodynamic-center positions from subsonic to supersonic speeds of approximately $0.13 \bar{c}$ for the complete wing or exposed wing panels was about the same as that for the similar wing of reference 2, although the positions were apparently farther forward for the flight model.

Dynamic Longitudinal Stability

Experimental values of the dynamic-longitudinal-stability factor ($C_{mq} + C_{m\dot{\alpha}}$), determined for the total configuration by the method presented in reference 4, are shown in figure 12 as a function of Mach number. The variation of ($C_{mq} + C_{m\dot{\alpha}}$) with Mach number is large, but similar variations are common in the transonic speed range (ref. 7). The general level of the data is in agreement with values estimated for just the fuselage plus the tail using the tail lift-curve slopes presented in reference 4, and the effective downwash values from reference 8.

An attempted estimate of the wing contribution to the pitch damping did not explain the difference in variation with Mach number between the experimental values and estimated values for the fuselage plus tail. The estimated contribution of the wing for subsonic speeds was very slight for the center-of-gravity position of 0.094 \bar{c} forward of the leading edge of the mean aerodynamic chord. For the low supersonic speeds and wing plan form of this investigation the methods of reference 9 are not strictly applicable, but indicate that the wing contribution would be small.

Loading Distribution Over Fuselage

The distributions of loading on the fuselage in the vicinity of the wing are presented in figure 13. The data represent the difference in pressure coefficient between corresponding orifices on the top and bottom of the fuselage. These loading distributions in the vicinity of the wing were used with the exposed-wing data to obtain the complete-wing data. For the small angle-of-attack range of the tests the variation in loading from the center line to the 45° position is quite small for most chordwise stations.

SUMMARY OF RESULTS

A free-fall test at transonic speeds and small angles of attack of a low-aspect-ratio 45° sweptback wing and a 45° swept horizontal tail located in the extended wing-chord plane has yielded the following results:

1. The lift-coefficient curves were linear, with a peak value of the lift-curve slope for the complete wing of 0.075 which occurred at a Mach number of 0.94.
2. Throughout the test Mach number range the variation of drag with lift for the complete wing was such that the inclination of the force

vector was roughly midway between theoretical values for an elliptical spanwise distribution of lift at subsonic speeds ($1/\pi A$) and for the resultant force vector perpendicular to the wing chord ($\frac{1}{57.3} C_{L_{\alpha W}}, C_{L_{\alpha W}}$ from experimental data).

3. The aerodynamic center shift of the complete wing or exposed wing panels, which occurred as the model traversed the transonic speed range, was about 13 percent of the mean aerodynamic chord and was approximately the same as that indicated by wind-tunnel data for a wing of the same plan form.

4. Tail contribution to longitudinal stability was small for the high subsonic Mach numbers, but increased tail effectiveness at the supersonic Mach numbers produced a large rearward shift on the aerodynamic center of the wing-body-tail combination.

5. The general level of the damping-in-pitch parameter ($C_{m_q} + C_{m_{\dot{\alpha}}}$) was in agreement with calculations in which most of the damping was attributed to the horizontal tail surfaces.

Ames Aeronautical Laboratory
National Advisory Committee for Aeronautics
Moffett Field, Calif., Sept. 17, 1954

REFERENCES

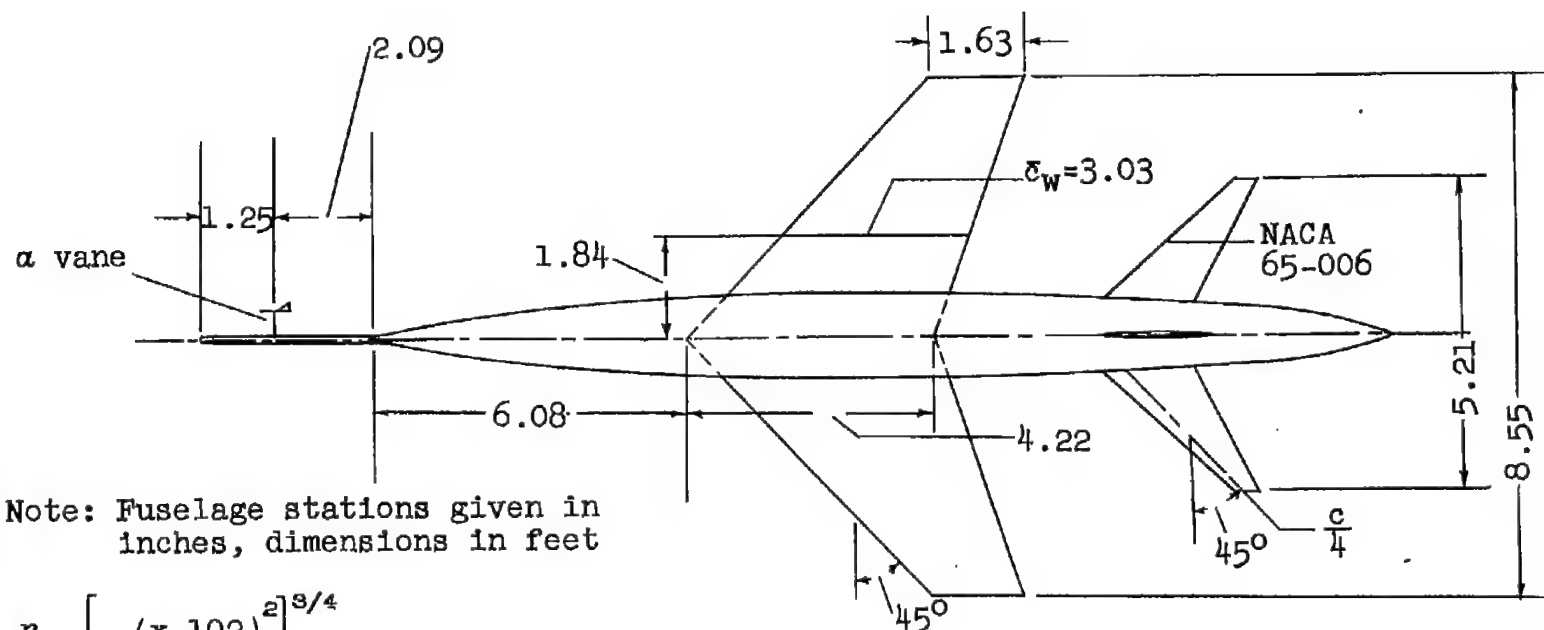
1. Heitmeyer, John C.: Lift, Drag, and Pitching Moment of Low-Aspect-Ratio Wings at Subsonic and Supersonic Speeds - Plane 45° Swept-Back Wing of Aspect Ratio 3, Taper Ratio 0.4 With 3-Percent-Thick, Biconvex Section. NACA RM A51H10, 1951.
2. Hall, Charles F.: Lift, Drag, and Pitching Moment of Low-Aspect-Ratio Wings at Subsonic and Supersonic Speeds. NACA RM A53A30, 1953.
3. Holdaway, George H.: Comparison of the Aerodynamic Characteristics at Transonic Speeds of a Plane Wing and a Cambered and Twisted Wing, Both Having 45° of Sweepback and an Aspect Ratio of 6. NACA RM A53B16, 1953.
4. White, Maurice D.: Effect of Camber and Twist on the Stability Characteristics of Models Having a 45° Swept Wing as Determined by the Free-Fall Method at Transonic Speeds. NACA RM A52F16, 1952.
5. White, Maurice D.: A Flight Investigation at Transonic Speeds of the Aerodynamic characteristics of a Model Having a Thin Unswept Wing of Aspect Ratio 3.1. NACA RM A54E12, 1954.

6. Holdaway, George H.: Comparison of Theoretical and Experimental Zero-Lift Drag-Rise Characteristics of Wing-Body-Tail Combinations Near the Speed of Sound. NACA RM A53H17, 1953.
7. Gillis, Clarence L., and Chapman, Rowe, Jr.: Summary of Pitch-Damping Derivatives of Complete Airplane and Missile Configurations as Measured in Flight at Transonic and Supersonic Speeds. NACA RM L52K20, 1953.
8. Coppolino, Domenic A.: The Effective Downwash Characteristics at Transonic Speeds of a 6-Percent-Thick Wing with 47° of Sweepback in Combination With a Cylindrical Body as Determined from Force Measurements of a Horizontal Tail. NACA RM L52J15, 1952.
9. Malvestuto, Frank S., Jr., and Hoover, Dorothy M.: Lift and Pitching Derivatives of Thin Sweptback Tapered Wings with Streamwise Tips and Subsonic Leading Edges at Supersonic Speeds. NACA TN 2294, 1951.

TABLE I.- PHYSICAL CHARACTERISTICS OF TEST MODEL

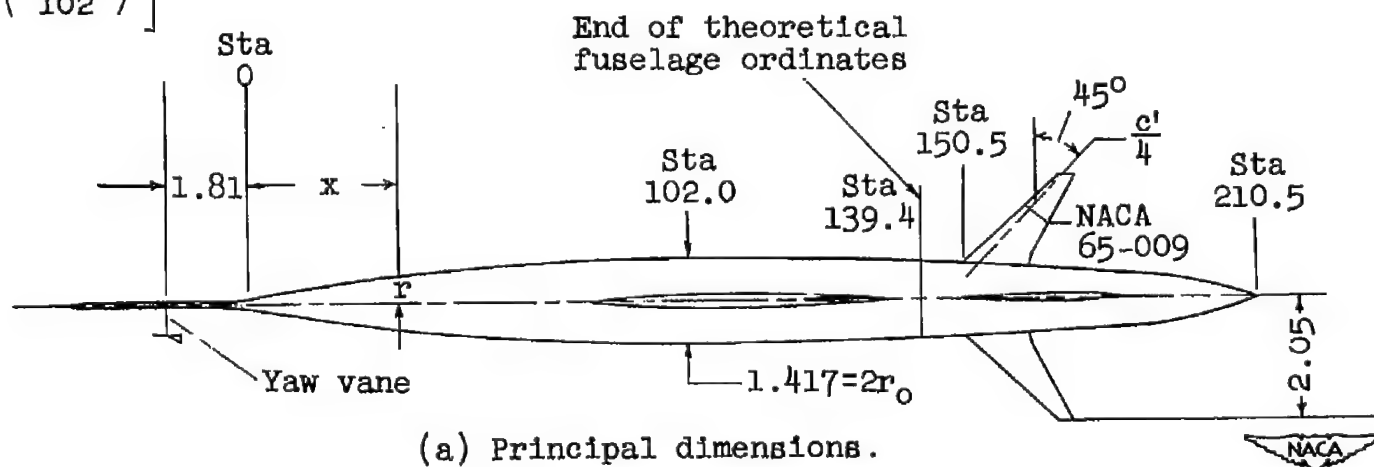
Wing		
Area, sq ft		24.5
Aspect ratio		3.0
Taper ratio		0.4
Mean aerodynamic chord, ft		3.03
Airfoil sections	NACA 64A006 perpendicular to the line of their own 0.25 chords ($c'/4$)	
Sweep of $c'/4$ line, deg		39.5
Sweep of leading edge, deg		45.0
Fuselage		
Fineness ratio		12.4
Maximum diameter, in.		17.0
Nose boom diameter, in.		1.50
Fuselage radii at stations behind the theoretical ordinates		
	<u>Fuselage station</u>	<u>Inches</u>
	140.0	7.23
	150.0	7.10
	160.0	6.60
	165.0	6.34
	189.6	5.10
	195.6	4.50
	201.6	3.20
	204.6	2.30
	210.5	0
Horizontal tail surfaces		
Area, sq ft		6.0
Aspect ratio		4.5
Taper ratio		0.2
Airfoil section	NACA 65-006 streamwise	
Sweep of streamwise 0.25 chord, deg		45.0
Vertical tail surfaces		
Area, sq ft		3.1
Aspect ratio		5.1
Taper ratio		0.22
Airfoil section	NACA 65-009 perpendicular to the line of their own 0.25 chords ($c'/4$)	
Sweep of $c'/4$ line, deg		45.0
General		
Weight, lb		1770
Center of gravity, forward of leading edge of \bar{c}		0.094 \bar{c}

REPRODUCED



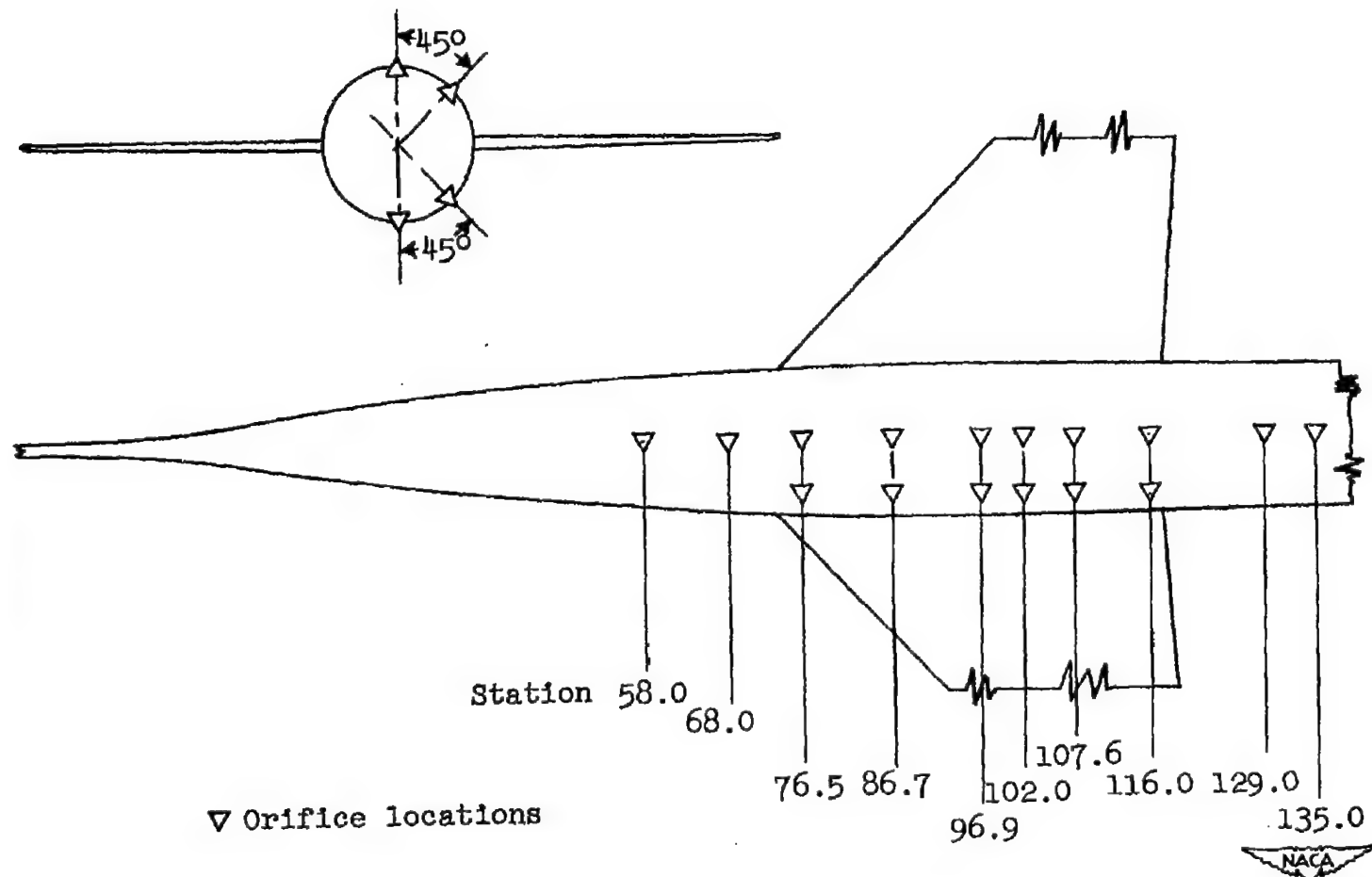
Note: Fuselage stations given in inches, dimensions in feet

$$\frac{r}{r_0} = \left[1 - \left(\frac{x-102}{102} \right)^2 \right]^{3/4}$$



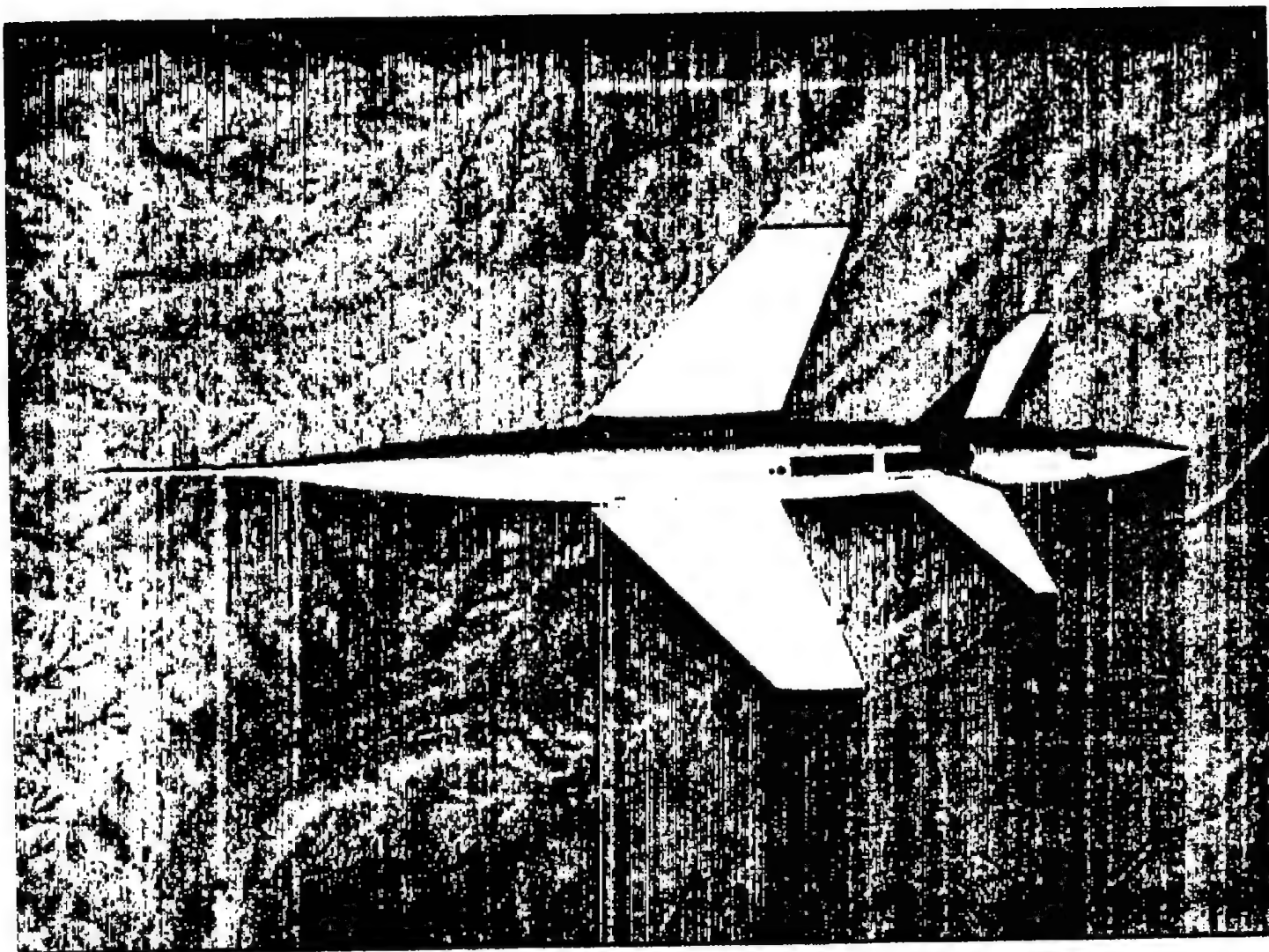
(a) Principal dimensions.

Figure 1.- Details of test model.



(b) Locations of pressure orifices on upper and lower surfaces of fuselage.

Figure 1.- Concluded.



A-19053

Figure 2.- Model in flight.

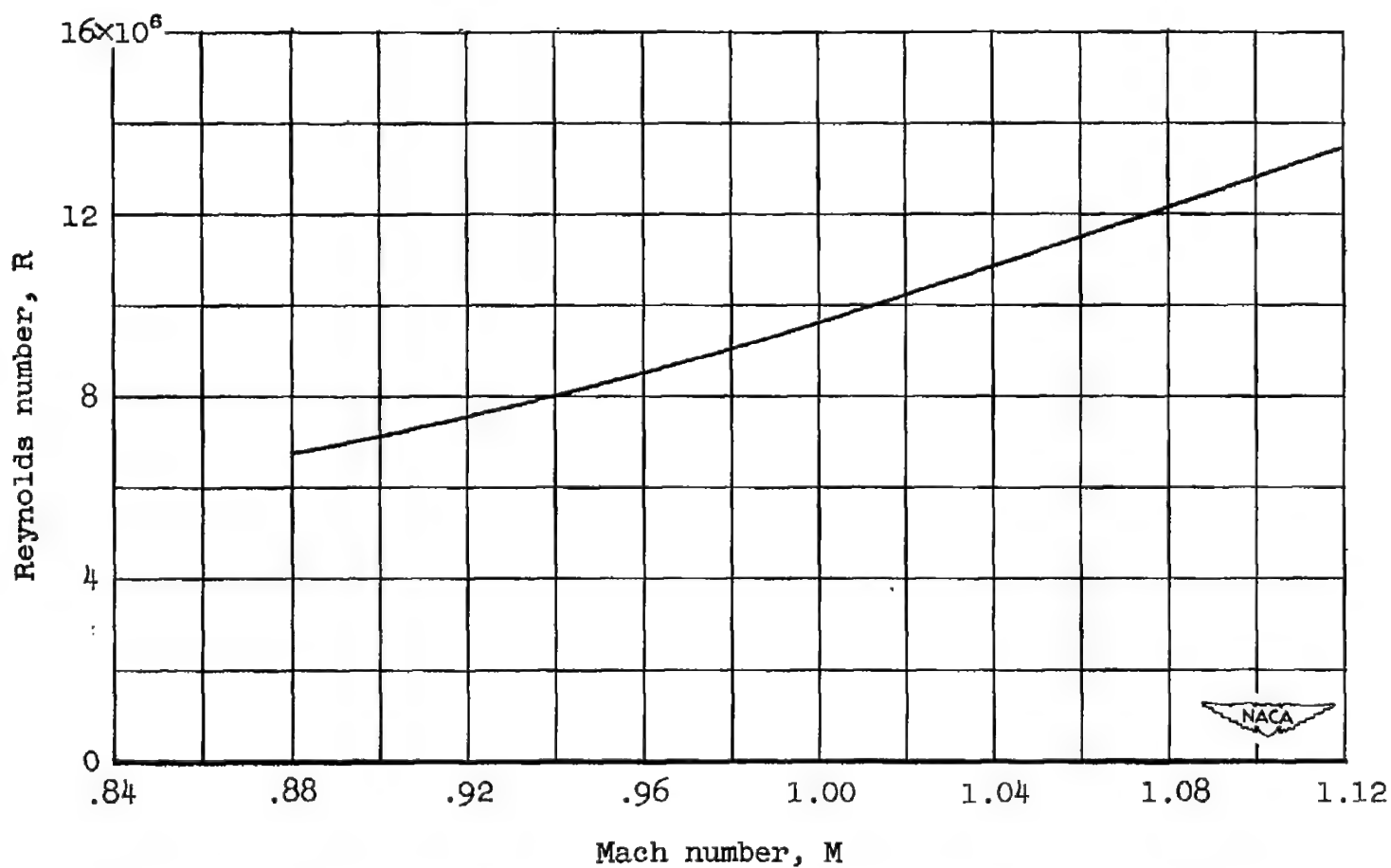
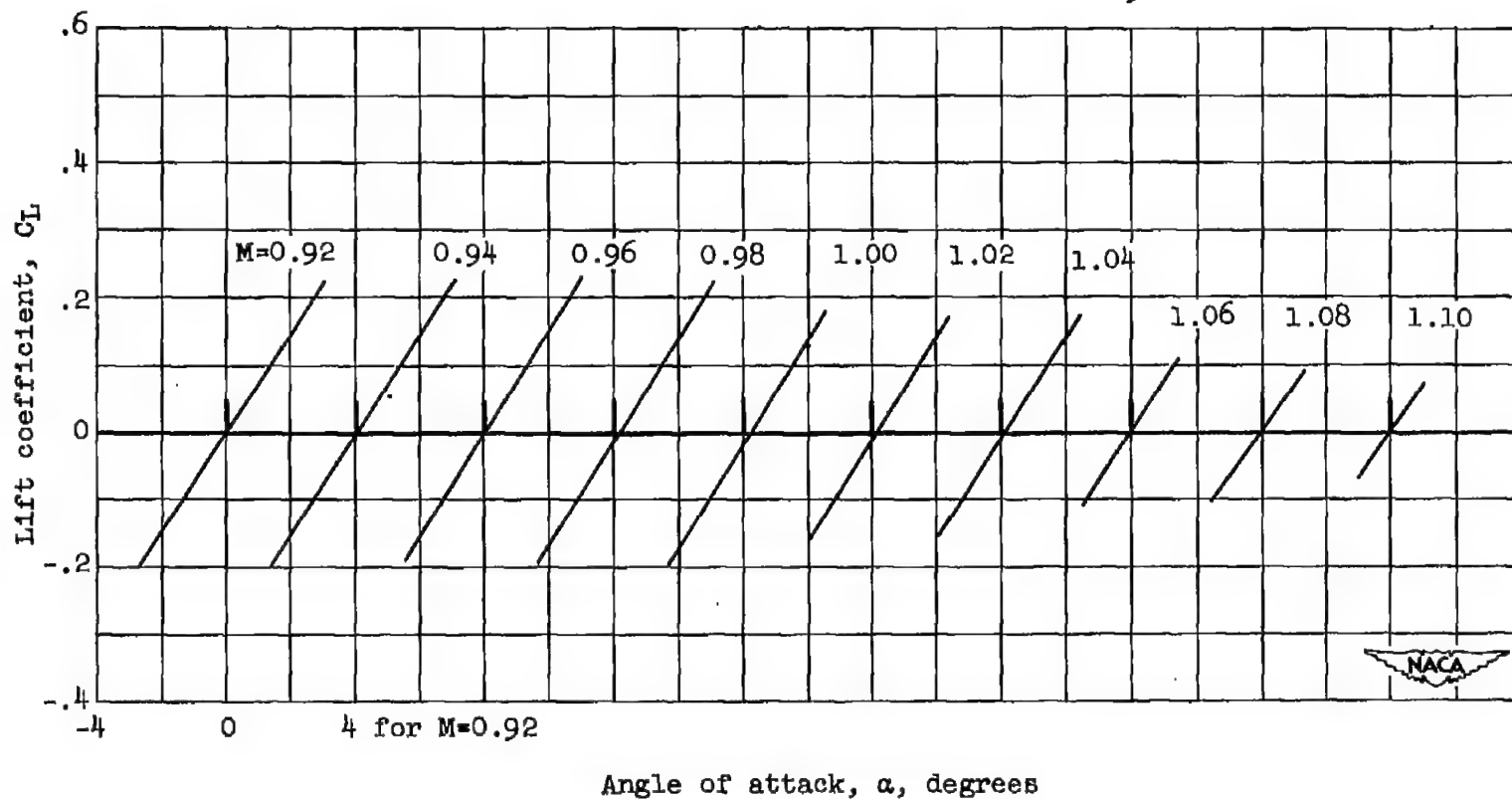
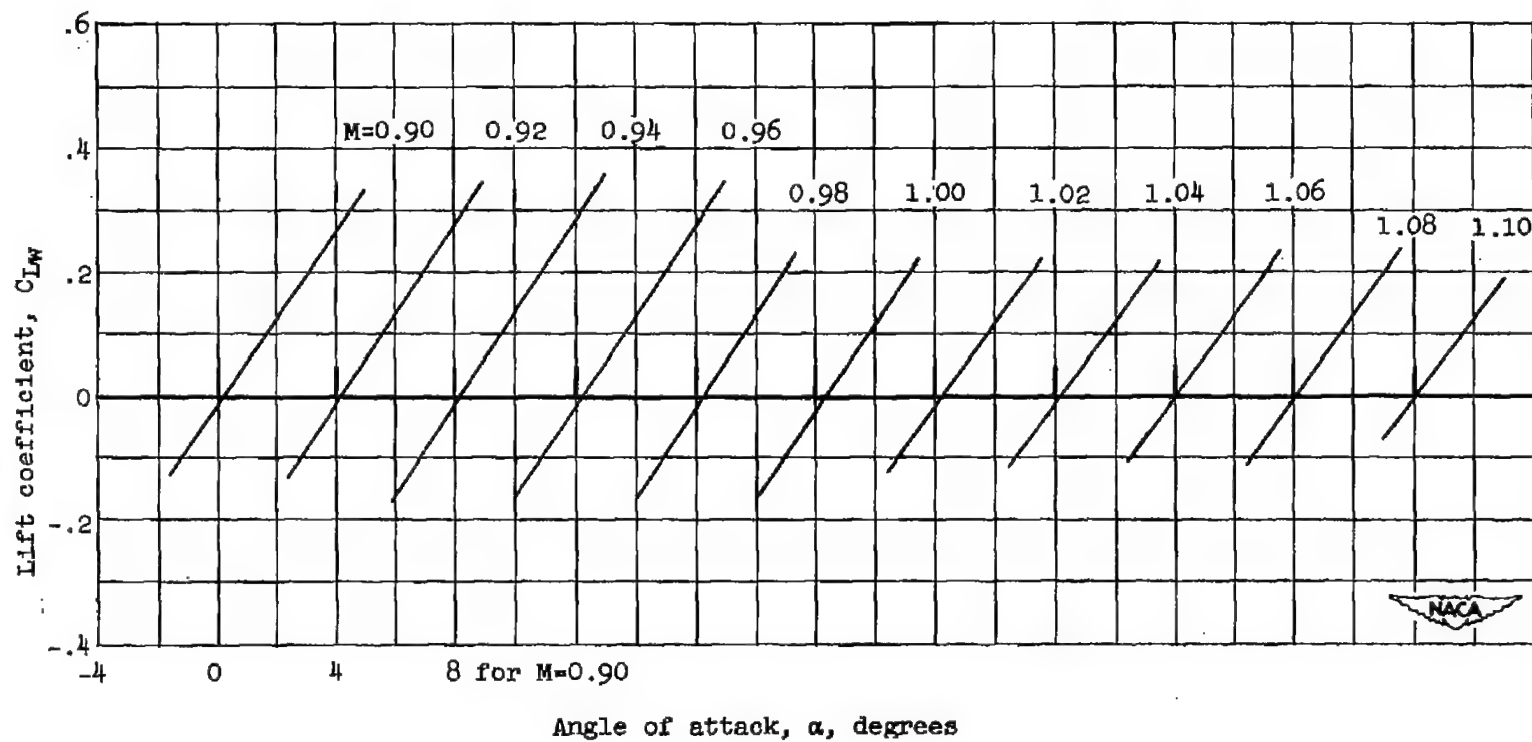


Figure 3.- Reynolds number variation with Mach number for the tests.



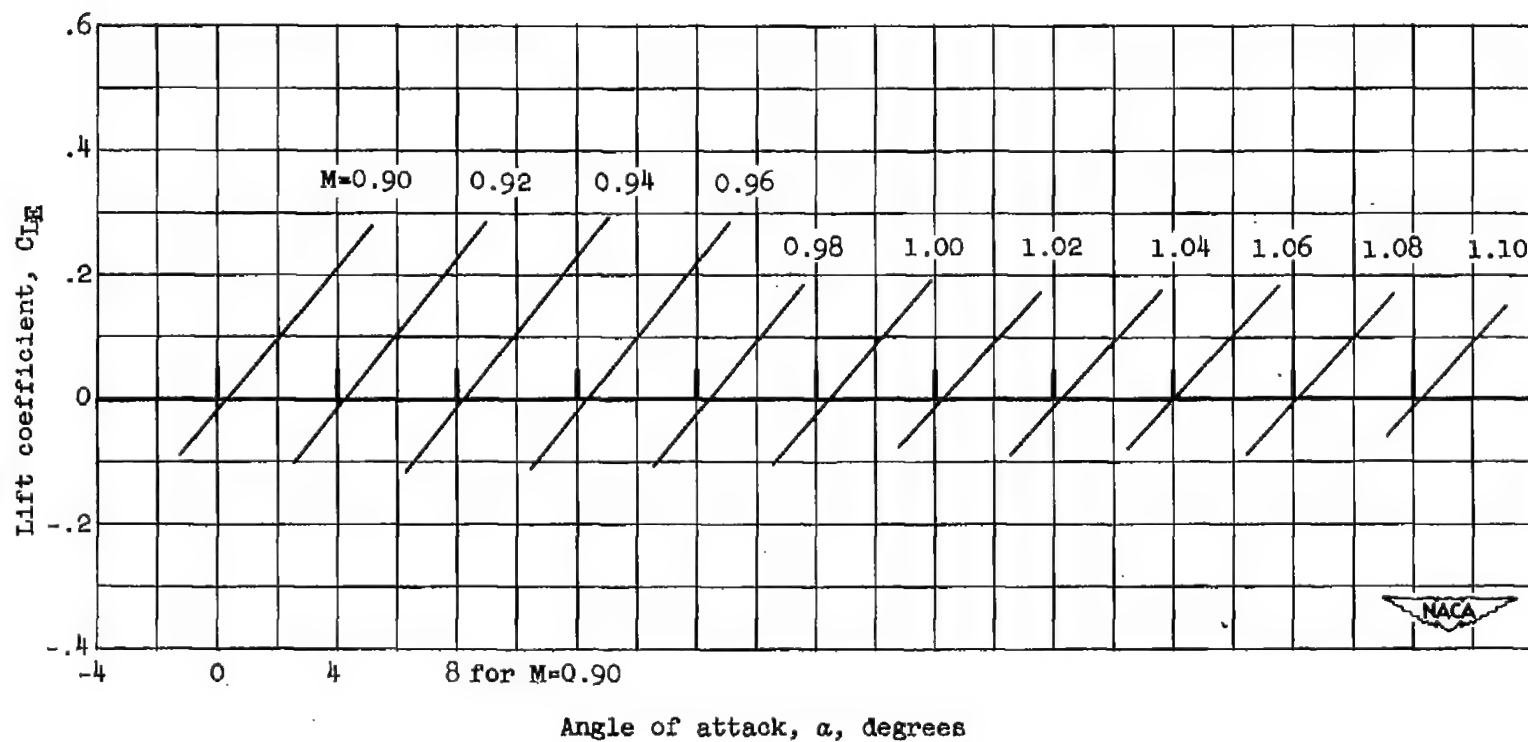
(a) Total configuration.

Figure 4.- Lift coefficient as a function of angle of attack at various Mach numbers.



(b) Complete wing.

Figure 4.- Continued.



Angle of attack, α , degrees

(c) Exposed wing panels.

Figure 4.- Concluded.

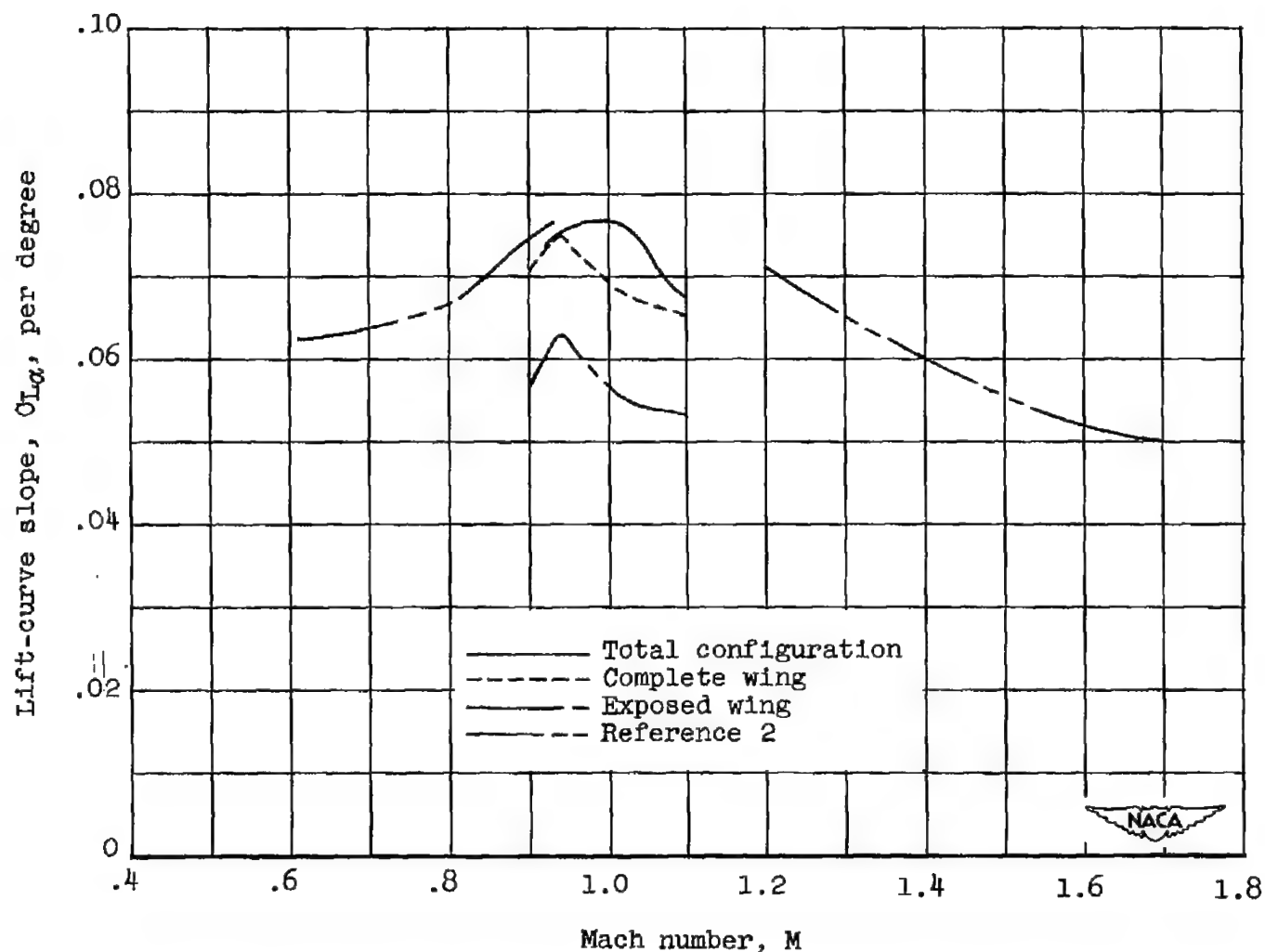
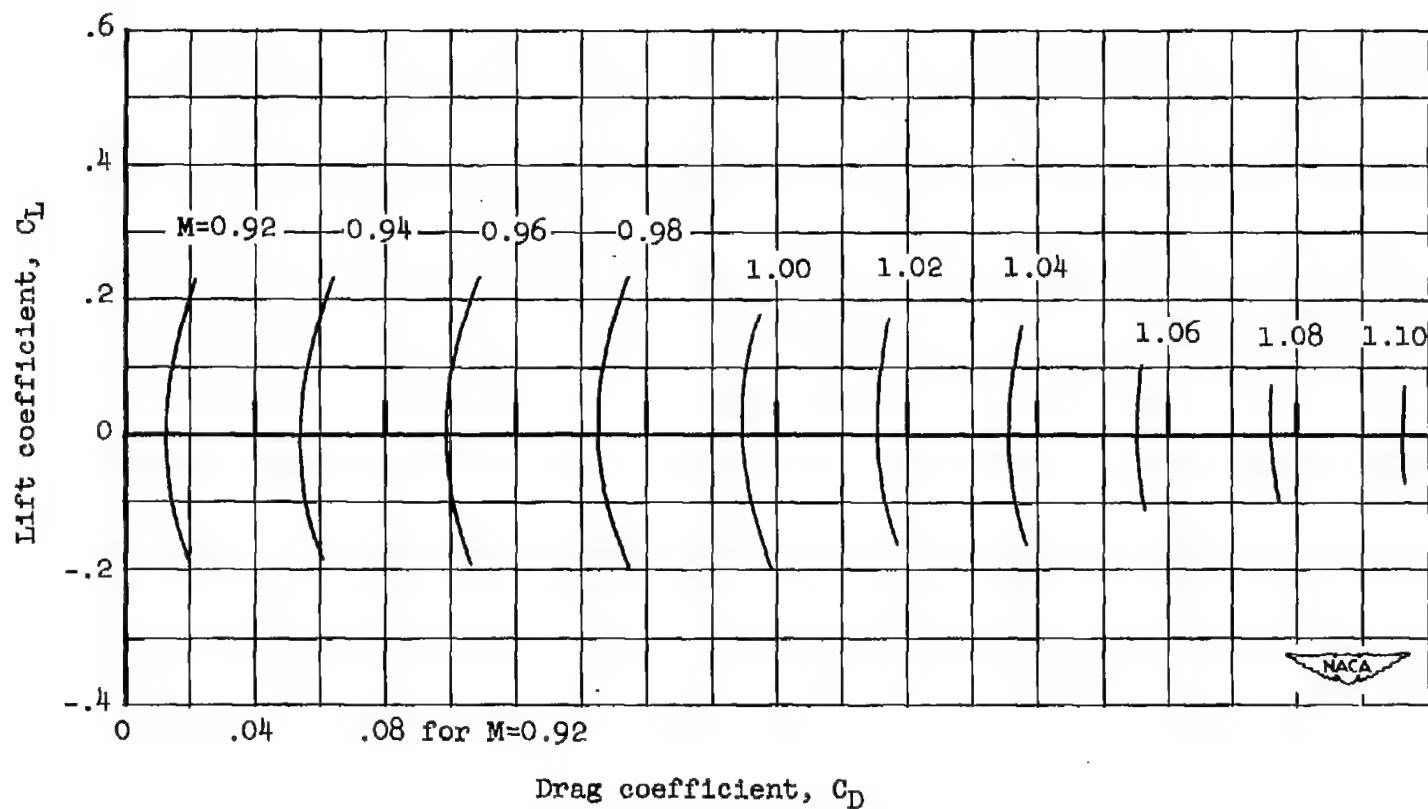
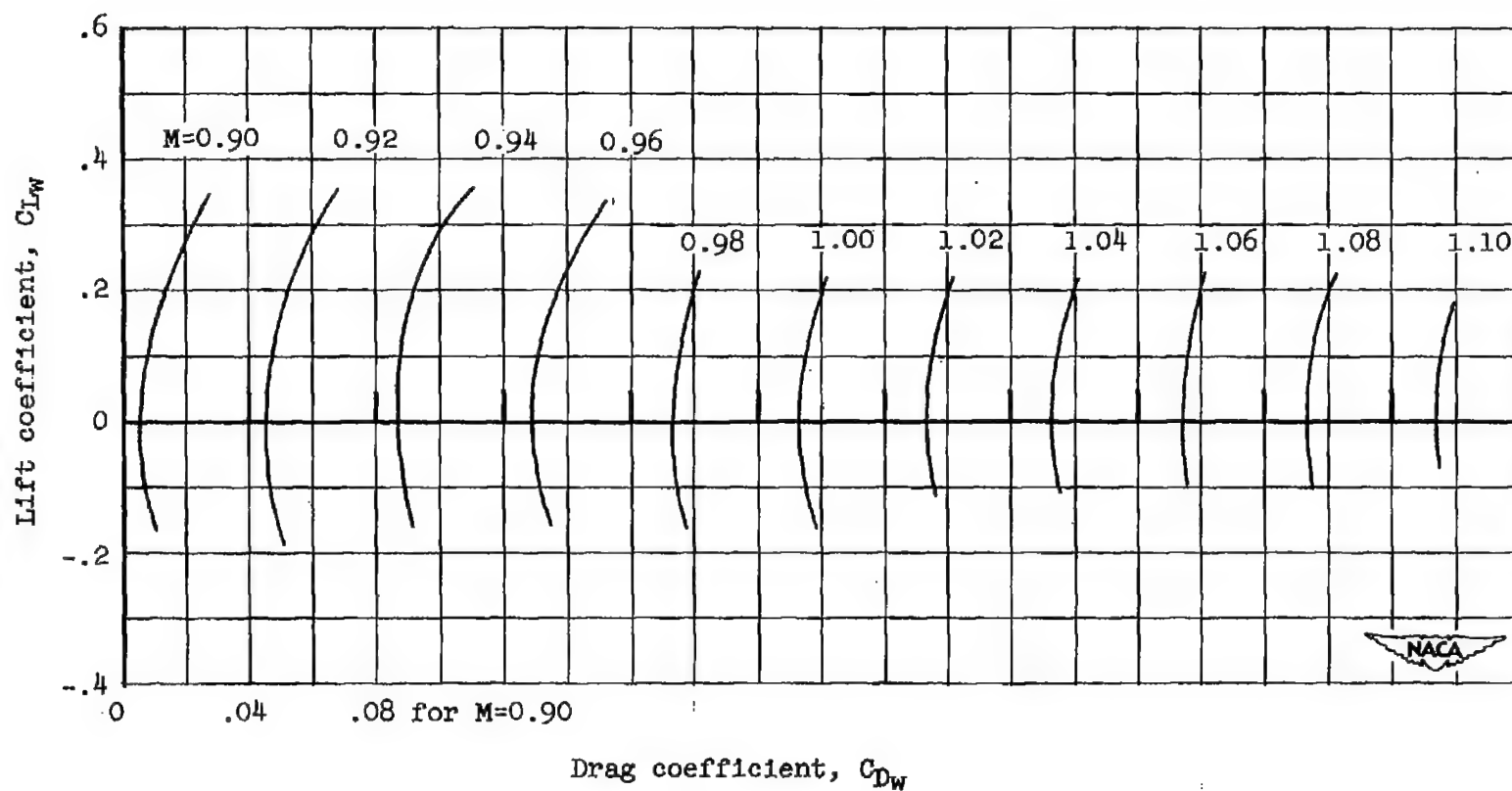


Figure 5.- The lift-curve slope for several components of the test model, and for a wing of the same plan form but with a 3-percent-thick biconvex airfoil section, reference 2.



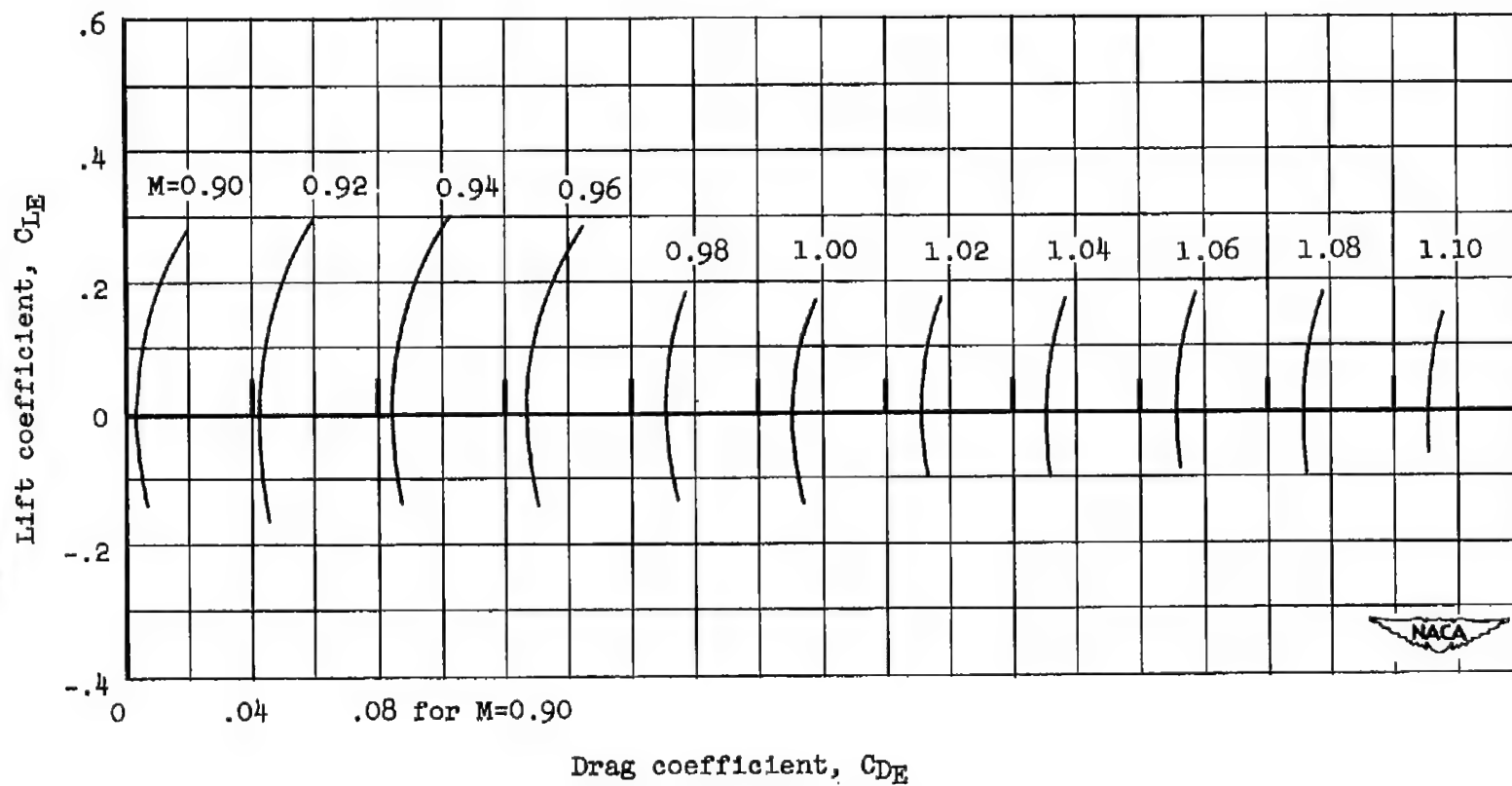
(a) Total configuration.

Figure 6.- Drag coefficient as a function of lift coefficient for various Mach numbers.



(b) Complete wing.

Figure 6.- Continued.



Drag coefficient, C_{DE}

(c) Exposed wing panels.

Figure 6.- Concluded.

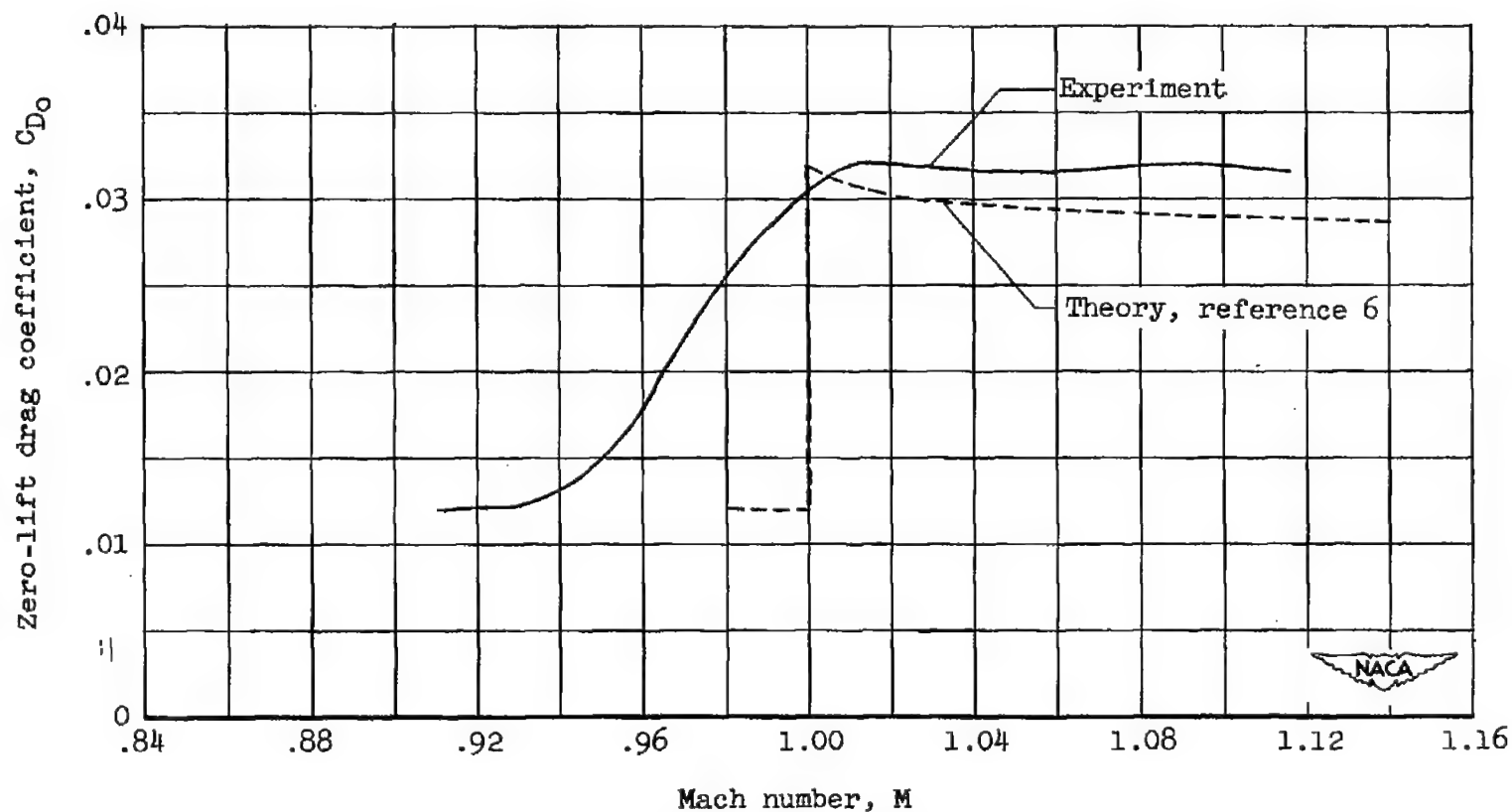


Figure 7.- Comparison of experimental zero-lift drag coefficients for the total configuration, with theoretical wave-drag coefficients added to the level of the experimental drag coefficients at subsonic speeds.

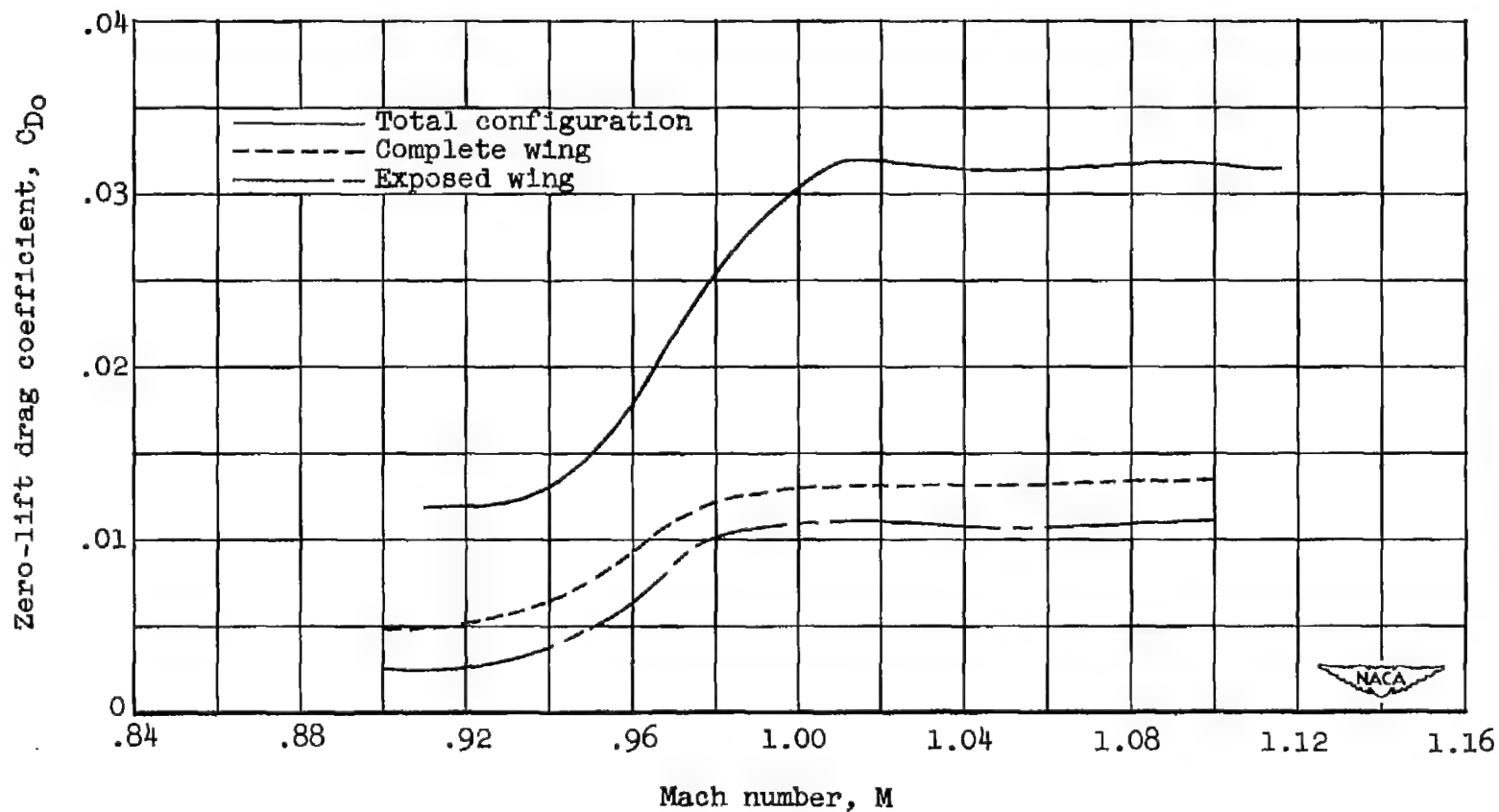


Figure 8.- The zero-lift drag coefficients for several components of the test model.

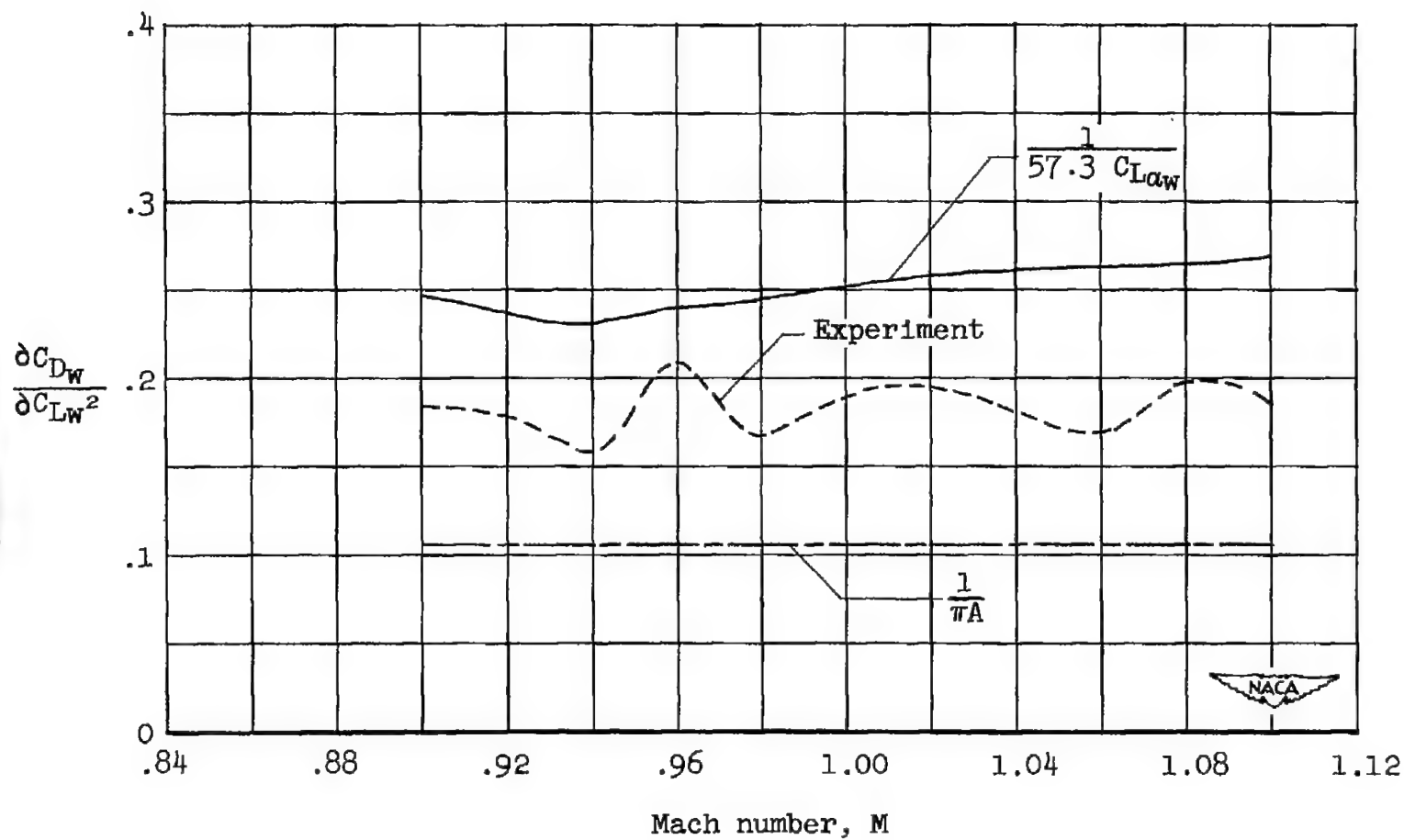
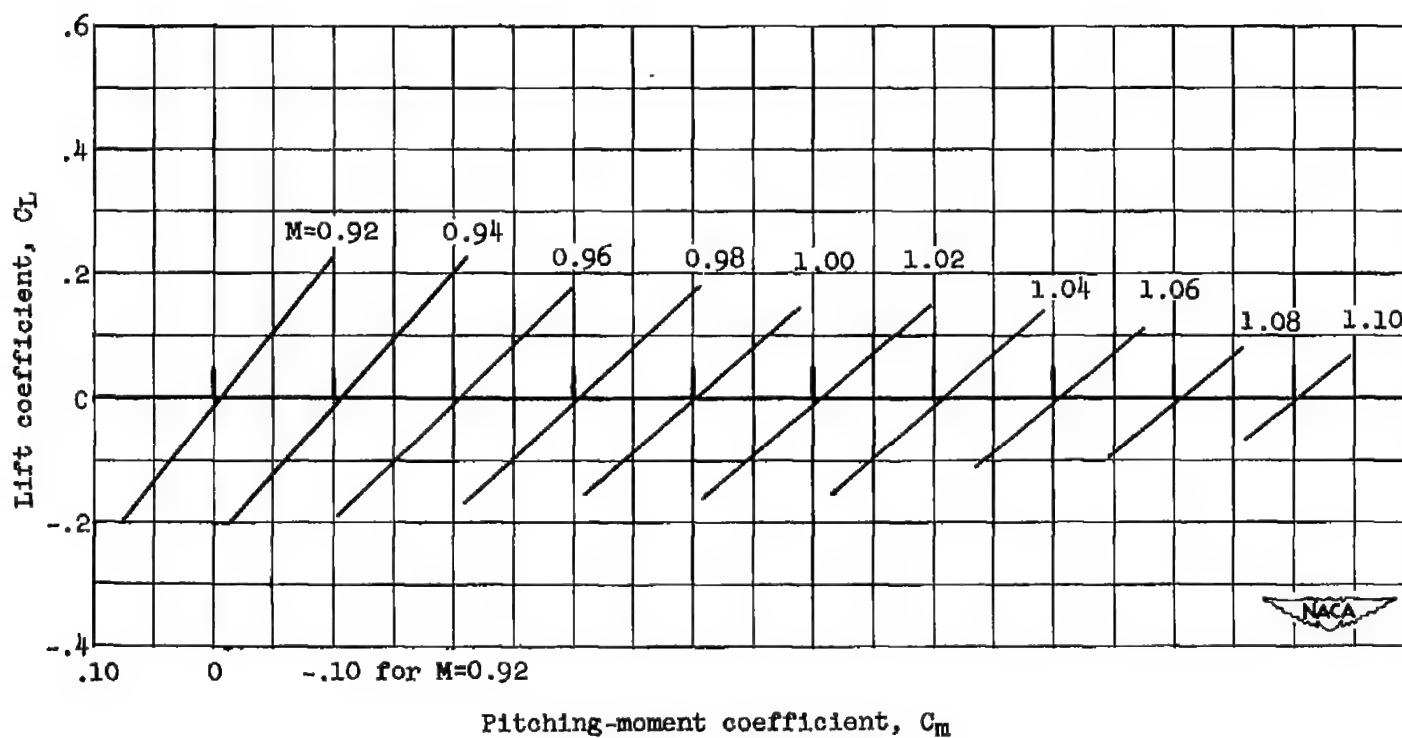
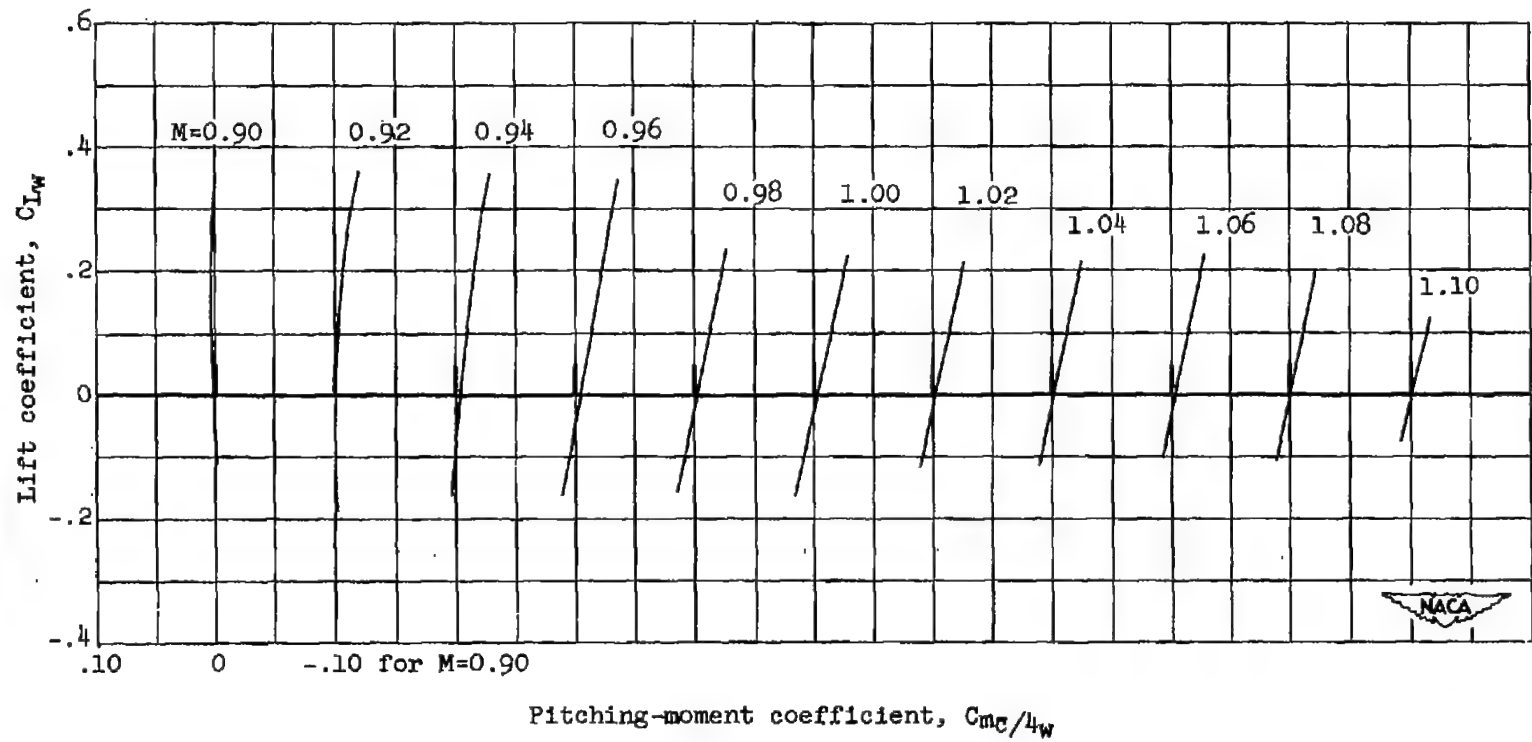


Figure 9.- The drag-rise parameter ($\partial C_{DW}/\partial C_{LW}^2$) for the complete wing.



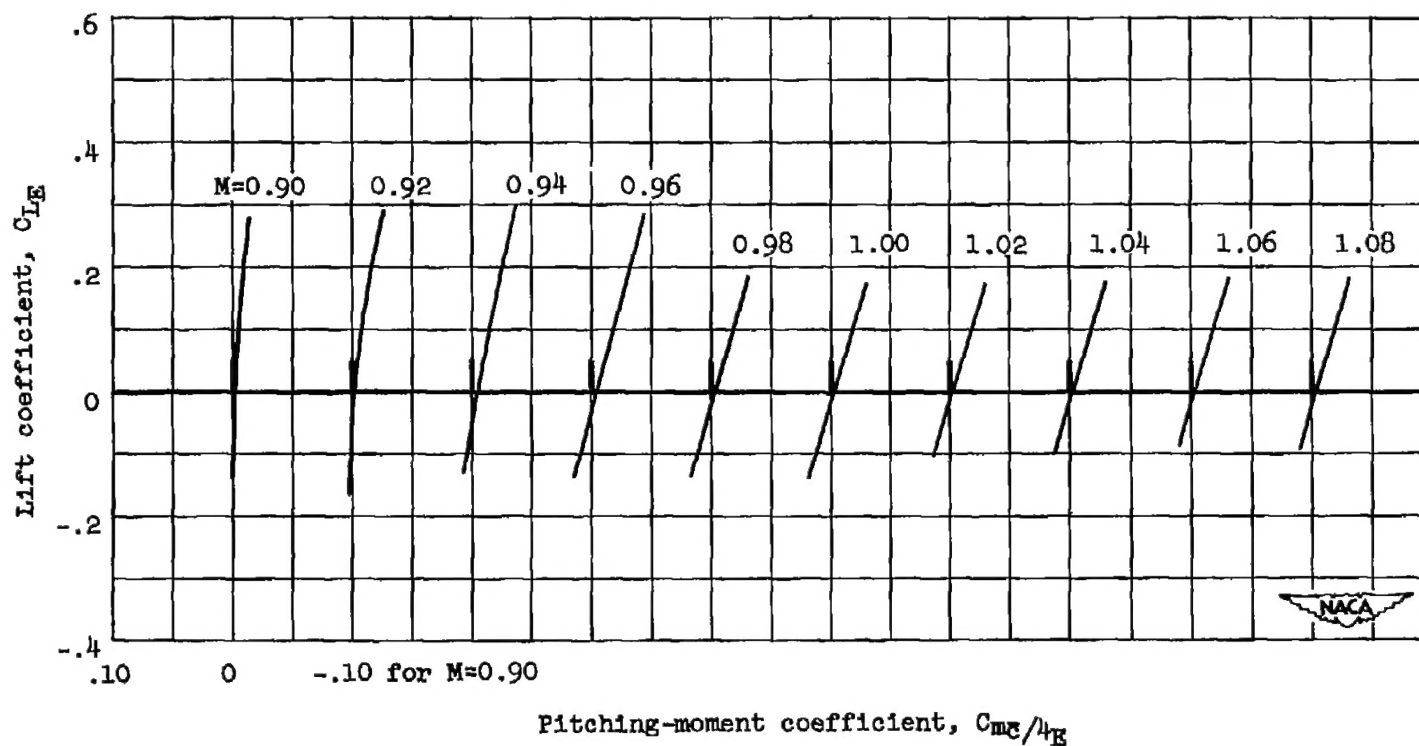
(a) Total configuration.

Figure 10.- Pitching-moment-coefficient variation with lift coefficient and Mach number.



(b) Complete wing.

Figure 10.- Continued.



(c) Exposed wing panels.

Figure 10.- Concluded.

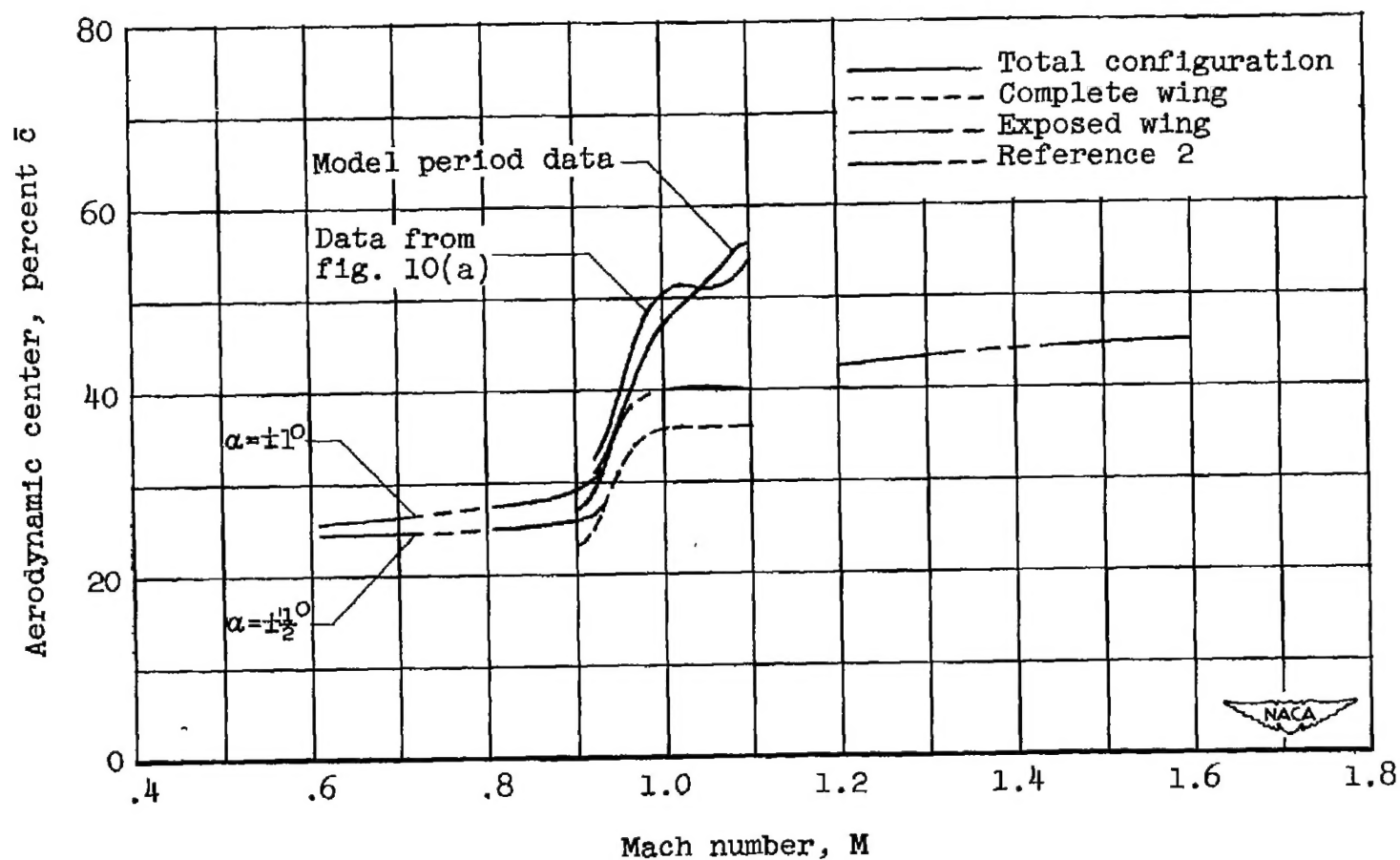


Figure 11.- The aerodynamic-center position for several components of the test model, and for a wing of the same plan form, reference 2.

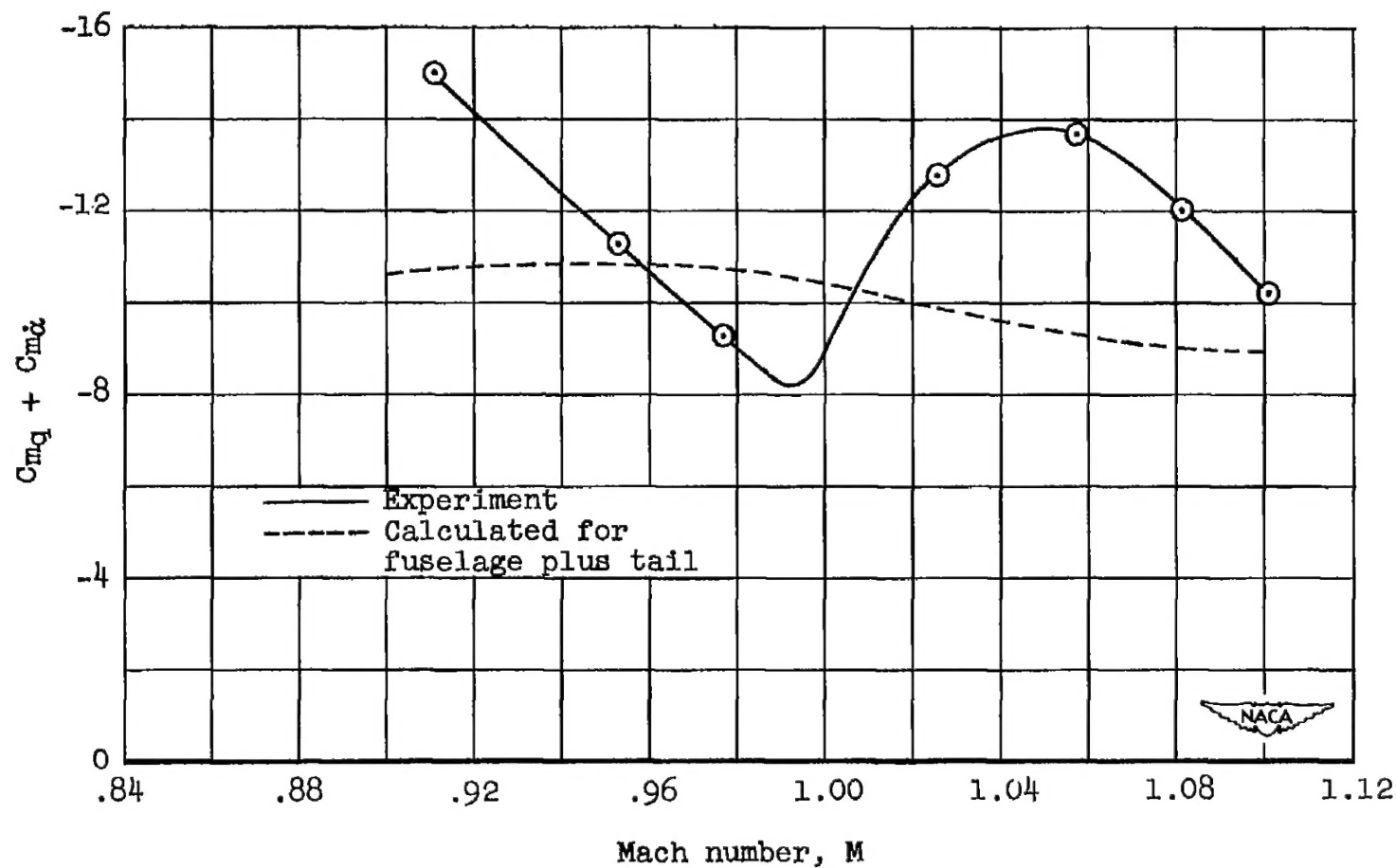


Figure 12.- The dynamic longitudinal stability ($C_{mq} + C_{m\dot{\alpha}}$) for the total configuration.

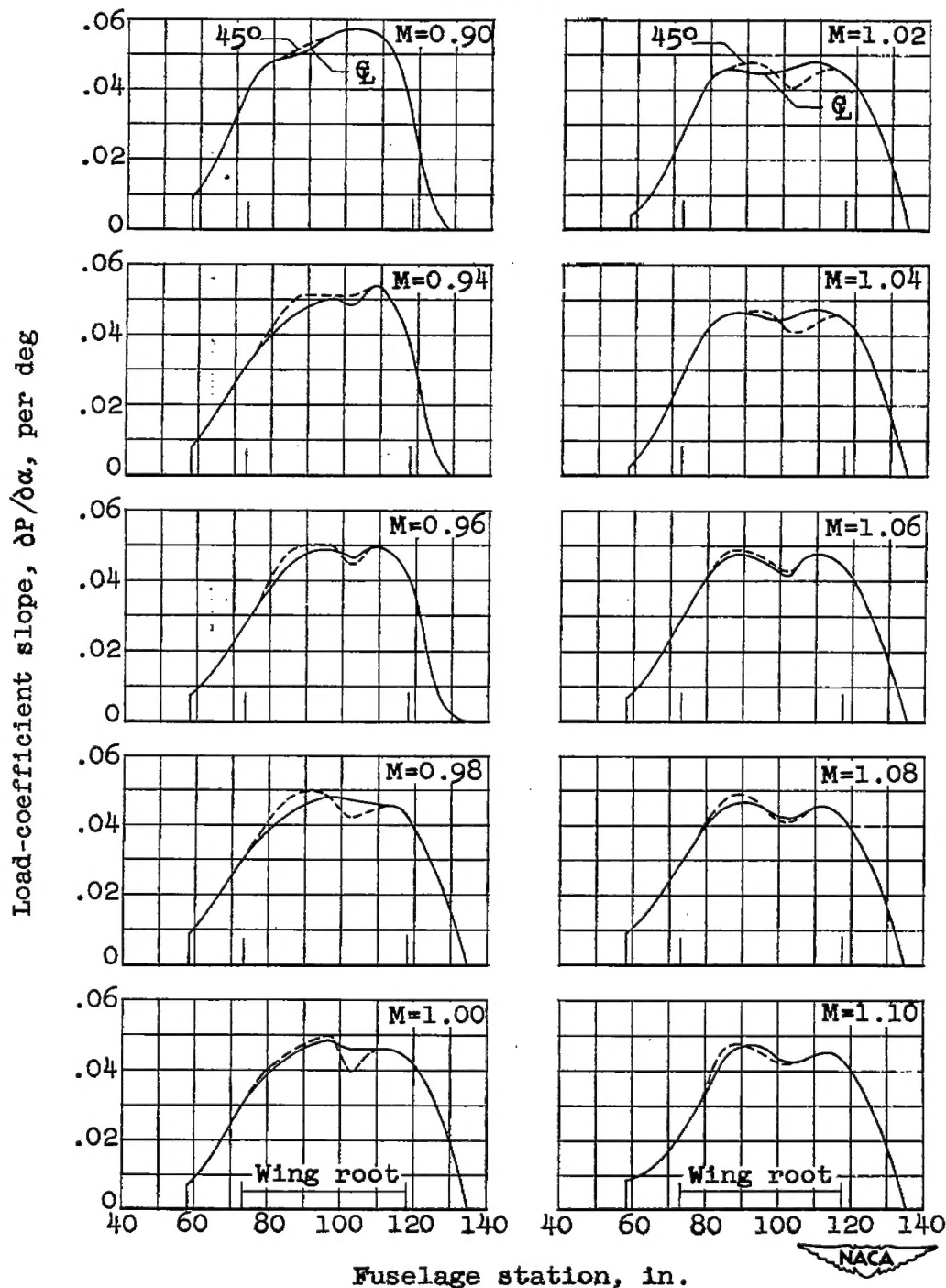


Figure 13.- Chordwise distributions of load-coefficient slope over the fuselage in the vicinity of the wing, for fuselage center-line orifices and orifices rotated 45° to the left (see fig. 1(b)).